Available online at www.sciencedirect.com
ScienceDirect
Journal of the European Ceramic Society 27 (2007) 511–516
www.elsevier.com/locate/jeurceramsoc

FEM simulations of microstructure effects on thermoelastic properties of sintered ceramics

M. Iuga *, F. Raether

Fraunhofer Institut Silicatforschung, Würzburg, Germany

Available online 24 May 2006

Abstract

A model was developed to simulate macroscopic material properties of polycrystalline ceramics from the material properties of the constituting phases and the microstructure. Cubic and random structures were included. The model allows a variation of volume fractions of the phases, grain size and grain boundary areas. Representative for a large number of material properties, elastic tensor, thermal conductivity, coefficient of thermal expansion and thermal stress are calculated for individual microstructures using finite element methods (FEM). Simulations focus on two types of bi-continuous ceramic composites: zirconia toughened alumina (ZTA) and a porous zirconia ceramic which was infiltrated by a spinel-glass. Microstructure of experimental samples is represented by two different model structures: a Voronoi type structure for the ZTA ceramic and a cubic structure of cubes interconnected by cylinders for the infiltrated zirconia system. A substantial impact of microstructure on macroscopic material properties and internal stress distribution is obtained. A good agreement between measured and simulated material properties was found.

Keywords: Composites; Microstructure-final; Thermal properties; Mechanical properties

1. Introduction

Predictive methods which allow an accurate simulation of composite properties from microstructure and material properties of its constituting phases would drastically increase efficiency in the development of novel ceramics. Therefore, microstructure–property relations were intensely investigated during the last 50 years. Whereas composites consisting of a matrix phase and inclusions could be satisfactorily simulated, bi-continuous microstructures require more accurate simulation methods.

To estimate the effective material properties of bi-continuous ceramics many analytical methods have been developed. Most of them are essential variants of the composite cylinder model[1] or self-consistent models.[2,3] In the last decades, effective media theories which sufficiently describe microstructures with inclusions or closed pores have been widely used.[4–6] Another class of theories are the well known variational bounds[7–9] which provide rigorous upper and lower bounds of composite properties from given properties of participating phases.

The analytical models represent two-phase or multiphase materials only approximately, as they ignore specific details of the microstructure. To overcome this serious problem, numerical methods were developed using the increasing computer power. Among them finite element methods (FEM) are the most flexible numerical techniques. However, in many numerical studies, the microstructure to be analysed has been restricted to two dimensions or was approximated by periodic arrays of very simple items such as spheres or cylinders.[10,11]

In the present work, effective thermoelastic properties of two types of bi-continuous ceramic materials are studied exemplarily using 3d FEM models: zirconia toughened alumina (ZTA) and a zirconia ceramic which was infiltrated by a glass. The ZTA ceramic investigated is used as substrate in microelectronic industry due to its high fracture toughness.[13] The infiltrated ceramic is used in dental applications where it is excellently machinable by CAD/CAM.[14]

2. Experimental methods

The infiltrated ceramic was prepared by cold isostatic pressing of a zirconia powder, which was partially stabilised by 11% CeO_2, and sintering of the green compacts to 77 and 88% of theoretical density, respectively. Then the porous ceramic was

* Corresponding author. Tel.: +49 931 41 00 2 13; fax: +49 931 41 00 2 99.
E-mail address: maria.iuga@isc.fraunhofer.de (M. Iuga).

0955-2219/$ – see front matter © 2006 Elsevier Ltd. All rights reserved.
doi:10.1016/j.jeurceramsoc.2006.04.072

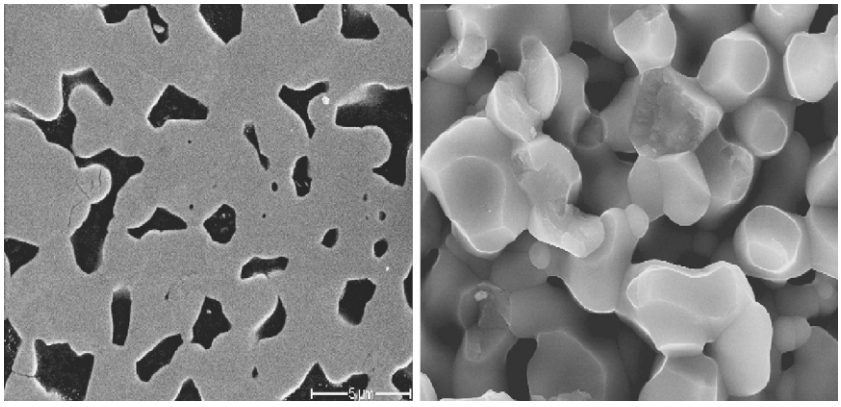

Fig. 1. SEM image of porous zirconia before infiltration: polished section (left) and fracture surface (right).

Table 1
Experimental data for the infiltrated ceramics and the constituting zirconia and spinel-glass phase: volume fraction of zirconia f_{s0}, Young's modulus E, Poisson's ratio ν, residual porosity f_p and CTE

Sample	f_s (%)	E (GPa)	ν	f_p (%)	CTE (10^{-6} 1/(K^{-1}))
Spinel-glass	0	85[14]	*0.22*	0	6.4[14]
zirconia 1	77[14]	180[16]	*0.22*	23[14]	12.2[14]
zirconia 2	88[14]	180[16]	*0.22*	12[14]	12.2[14]
Spinel-glass + zirconia 1	77[14]	154[14]		0–1[14]	11.2[14]
Spinel-glass + zirconia 2	88[14]	152[14]		3[14]	11.4[14]

Data obtained from literature are indicated by citation number; estimated data are in italic letters.

infiltrated by a spinel-glass at temperatures around 1100 °C to form a nearly dense composite of high strength. Experimental details are given. [14] Fig. 1 shows a fractured surface and a polished section of the porous zirconia ceramic before infiltration obtained by scanning electron microscopy (SEM, Hitachi S800, Japan). Microstructure is inhomogeneous and agglomerates were formed which are connected by unevenly distributed zirconia bridges. Microstructure did not change after infiltration of the spinel-glass (apart form the substitution of the pores by the spinel-glass.[14] Experimental data used for the simulation of the infiltrated ceramics are summarised in Table 1.

The ZTA ceramic was made by tape casting a slurry of alumina and zirconia powder and subsequent sintering to nearly theoretical density. In this case, zirconia was partially stabilised by 10 mol% Y_2O_3 and the ratio between zirconia and alumina was varied, i.e. samples ZTA1, ZTA2, ZTA3 with 60, 78, 85% Al_2O_3, respectively. Experimental details are given in literature.[13] Microstructure of a polished and thermally etched section of the ZTA ceramic is shown in Fig. 2. Zirconia can be distinguished from alumina by its darker colouring. Curvature of the grain boundaries is small. The average chord length of the alumina and zirconia grains was determined from the SEM images.[15] From the SEM images also the interfaces between ZrO_2 and ZrO_2 grains, Al_2O_3 and Al_2O_3 grains and ZrO_2 and $Al2O_3$ grains were determined from the number of intersections of random lines with the respective type of grain boundaries.[15] Some hundred grains were considered with each type of sample.

Thermal diffusivity of the ZTA samples was measured with the laser–flash method.[20] The samples were measured at room temperature. The thermal diffusivity values were determined by averaging 10 individual measurements. Measuring uncertainty (1 σ) was 4%. From thermal diffusivity α, thermal conductivity λ is calculated according to:

$$\lambda = \rho c_p \alpha \quad (1)$$

where ρ is the density and c_p is the specific heat of the sample (c_p of the composite was calculated by a rule of mixtures). Densities of the ceramic samples and of the spinel-glass used for the infiltration were measured by the Archimedes method. Porosity was determined by the difference between theoretical density calculated from the density of the participating phases and measured density.

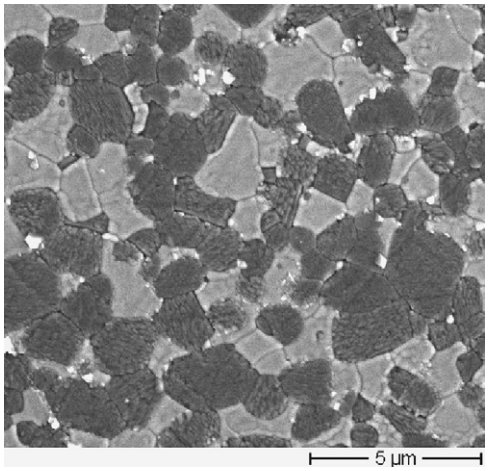

Fig. 2. SEM image of a polished section of a ZTA sample.

Table 2
Experimental data for the ZTA ceramics and the constituting alumina and zirconia phase: volume fraction of zirconia f_s, residual porosity f_p, density ρ, specific heat c_p, thermal conductivity λ, Young's modulus E and Poisson's ratio ν

Sample	f_s (%)	f_p (%)	ρ (g/cm^3)	c_p (J/(g K))	λ (W/(m K))	E (GPa)	ν
Al_2O_3	0	0	3.99[19]	0.78[19]	29[13]	390[19]	*0.22*
ZrO_2	0	0	5.94[18]	0.46[18]	3.1[13]	220[18]	0.3[18]
ZTA 1	60	1.94	4.68	0.61	11.09	277.94	
ZTA 2	78	3.99	4.25	0.68	21.67	339.44	
ZTA 3	85	1.09	4.22	0.71	22.79	359.98	

Data obtained from literature are indicated by citation number; estimated data are in italic letters.

Young's modulus of the ZTA samples was determined by ultrasonic velocity measurements (USIP12, Krautkramers, Hürth, Germany). Young's modulus E was calculated with formula:

$$E = \frac{(1+\nu)(1-2\nu)}{(1-\nu)}\rho c_l^2 \quad (2)$$

where ν is the Poisson ratio, ρ the sample density and c_l is the longitudinal ultrasonic velocity. Measuring uncertainty of Young's modulus measurement was 3%. Experimental data used for the simulation of the ZTA ceramics are summarised in Table 2.

3. The computational approach

A three dimensional model to simulate macroscopic properties of polycrystalline ceramics has been developed. Thermoelastic properties are calculated for cube shaped unit cells with periodic boundaries. Various microstructures are considered which are described in more detail in literature.[15] Among them, two special structures are used in the present paper. Since a quantitative three-dimensional description of the microstructure of the infiltrated ceramic is not possible (compare Fig. 1), it has been modelled by the simple cubic structure shown in Fig. 3. The bridges between the agglomerates have been considered by six cylindrical contacts to its six nearest neighbours. This structure allows a very large variation of contact area in comparison with other shapes,[12] by changing the radii of the cylinders. The area of the cylinder cross section is scaled by the area of the side face of the unit cell and is denoted a_s. The residual volume of the unit cell is attributed to the glass phase.

For the ZTA composite, a Voronoi model is used which can better describe two bi-continuous crystalline phases (compare Fig. 2). The microstructure is produced from a Poisson distribution of particle centres within the unit cell where the centre positions are obtained by a standard random number generator. The two phases are attributed randomly to the centre points according to their volume fractions and grain size ratio. The centre points are periodically continued in the neighbouring unit cells. Then the Voronoi tessellation is performed by constructing polyhedra which separate regions closest to each centre point. Actually a modification of this procedure based on radical planes is used to consider different grain sizes of the two phases. The algorithm is described in literature.[17] Typically 12 particle centres are used to generate one microstructure (Fig. 4). The measured microstructure parameters, i.e. volume fractions of the two phases, grain size ratio, and grain boundary areas are also calculated for each Voronoi structure. Then some hundred structures are generated and the structure which fits best to the respective experimental structure is selected for further simulation.

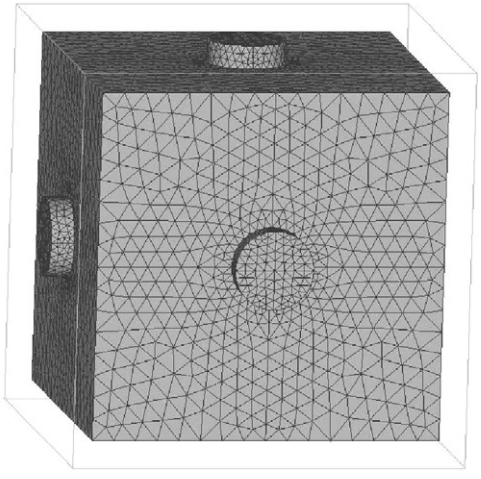

Fig. 3. Cubic structure (cube with six cylindrical contacts) used to describe the microstructure of the infiltrated ceramic (grey lines indicate the unit cell; the volume fraction of zirconia is 77%).

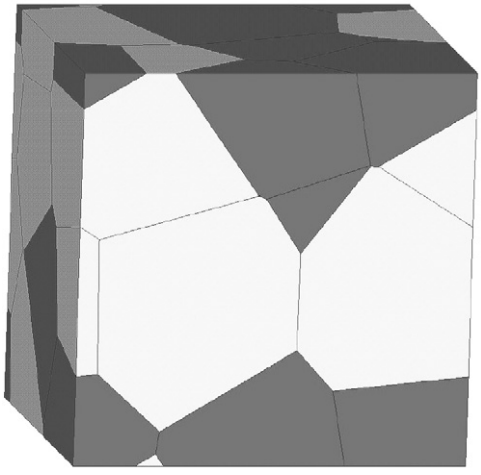

Fig. 4. Random structure (Voronoi polyhedra) used in the FE simulations for the ZTA ceramic (the volume fraction of zirconia is 50%).

Within the unit cell the material properties (thermal conductivity, Young's modulus, Poisson's ratio and coefficient of thermal expansion) are attributed to different phases and thermal and mechanical loads are applied. The constituent phases are assumed to be isotropic and linearly elastic. For thermal simulations, a temperature gradient is imposed on two opposite sides of the unit cell. The six independent elements of the symmetric thermal conductivity tensor are determined from the heat flow in three FE simulations using perpendicular temperature gradients and Fourier's law. For simulations of mechanical properties both tensile and shear strains are applied in different directions to determine the 21 independent elements of the symmetric stiffness matrix by Hook's law.[12]

Finally an additional simulation is performed to obtain material properties of an isotropic polycrystalline material. For that, the unit cell with its microstructure already simulated is replaced by a single hexagonal element of a homogenous anisotropic material. The overall properties of the unit cell are attributed to the material properties of the hexagonal element. Then a large cube is constructed from $20 \times 20 \times 20$ of such elements where the orientation of each element is determined from a random number generator. The material properties of the large cube are determined by applying loads as described for the small unit cell.[12]

The coefficient of thermal expansion (CTE) is obtained from the displacement of the faces of the unit cell after a change of uniform temperature. (The boundary conditions applied provide an equal displacement of the surface nodes in the direction perpendicular to the respective faces to maintain the cubic shape.) The resulting CTE is calculated as $(1/\Delta T) \times \Delta u$, where ΔT is the imposed temperature change and Δu represents the displacement which occur during the deformation.

4. Results and discussions

4.1. Spinel-glass in ZrO_2 ceramic

Fig. 5 shows the Young's moduli of the experimental samples which were measured with a zirconia volume fraction f_s of 0.77 and 0.88, respectively. Young's moduli are simulated varying a_s between 0.05 and 0.45 and f_s between 0.5 and 0.9. The effect of a_s on Young's moduli is smaller than 1%. Therefore, Fig. 5 shows simulated results for varying f_s only for $a_s = 0.20$. The numerical results for 77% ZrO_2 are in good agreement with the experimental data. However, for 88% ZrO_2 the simulated value of Young's modulus is higher than the experimental one. This effect is explained by the existence of 3% pores in the structure. In order to improve the FEM results, a subsequent simulation is performed where 3% spherical pores are introduced into a homogeneous material with the same elastic properties as the dense composite. Thereby the Young's modulus value decreases considerably and a good agreement between experimental and simulated values is achieved (Fig. 5).

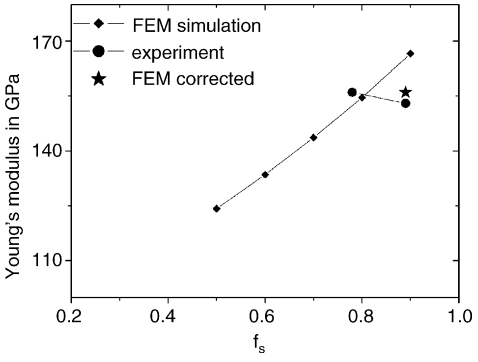

Fig. 5. Calculated Young's modulus for different volume fractions f_s of ZrO_2 and $a_s = 0.20$ together with experimental values.

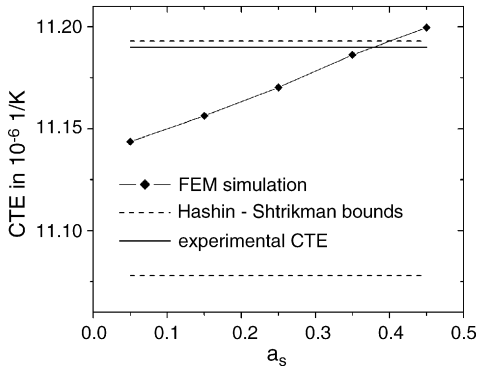

Fig. 6. Simulated coefficient of thermal expansion (CTE) as a function of contact area a_s together with the experimental value and the Hashin–Shtrikman bounds (77% ZrO_2 and 23% spinel-glass).

Fig. 6 shows that there is only a small increase of the simulated CTE with increasing a_s. The Hashin–Shtrikman bounds of the CTE[8] and the experimental CTE are also included in Fig. 6 for comparison with numerical calculations. It is seen that the simulated CTE values are essentially within the Hashin–Shtrikman bounds and agree to the experimental value.

Thermal stresses due to mismatch in thermal expansion between the spinel-glass and ZrO_2 are calculated by considering the cooling period after infiltration of the spinel-glass. Stresses form during the cooling period between 700 °C (transition temperature of spinel-glass) and 25 °C. Fig. 7 shows first principal stresses averaged for the respective phases with different values of a_s. As expected, the material with the larger value of the ther-

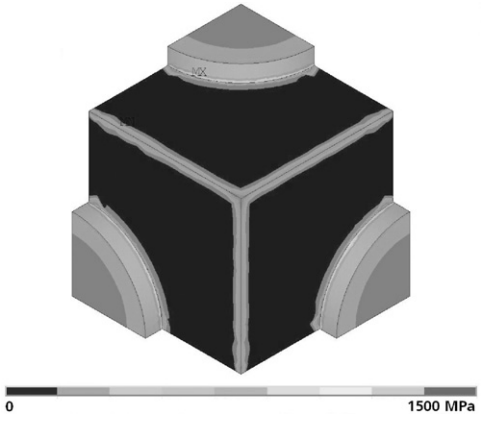

Fig. 7. Simulated 1st principal stresses for different values of contact areas a_s (77% ZrO_2 and 23% spinel-glass).

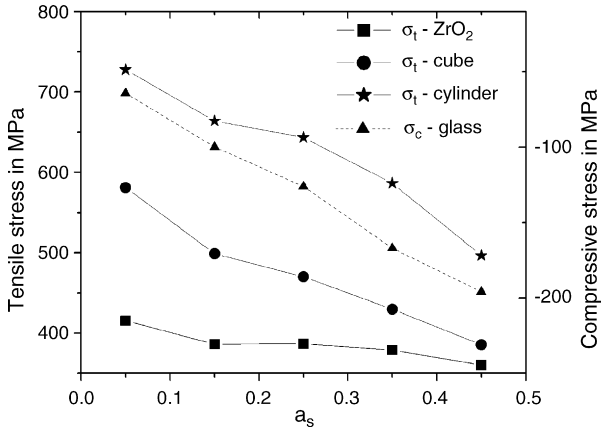

Fig. 8. Thermal stresses at the interface between ZrO_2 and spinel-glass within the unit cell for the infiltrated ceramic microstructures (78% ZrO_2 and 22% spinel-glass). σ_t and σ_c represent the tensile and compressive stress, respectively. The word cube stands for the faces of the cube and cylinder for the lateral surfaces of the cylindrical junctions between the particles.

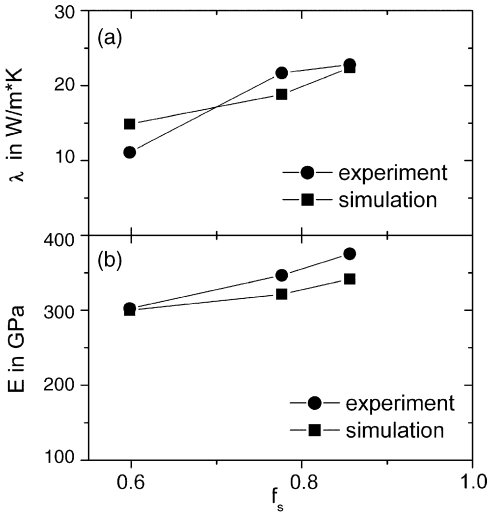

Fig. 10. Comparison of experimental and simulated thermoelastic properties of the ZTA ceramics: (a) thermal conductivities, λ and (b) Young's moduli, *E*.

mal expansion coefficient (ZrO_2) is subjected to a tensile stress and the spinel-glass is under compression. This was intended since the spinel-glass is the weaker component. Average tensile stresses at the interface between zirconia and spinel-glass are determined separately for the lateral surfaces of the cylindrical junctions between the agglomerates and for the faces of the cube (Fig. 8). It is seen that all tensile stresses decrease considerably with increasing cross section of the cylinders and the compressive stress in the glass phase increases. Therefore, best mechanical properties are expected when the junctions between the zirconia grains are maximised.

4.2. Zirconia toughened alumina

Fig. 9 shows a comparison of geometrical properties obtained from image analysis of the experimental samples and properties

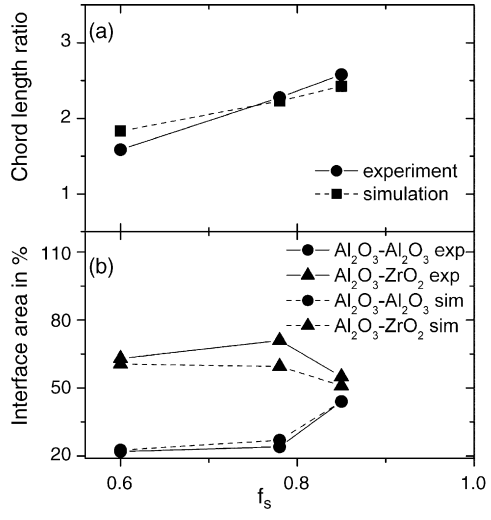

Fig. 9. Geometrical properties of microstructures derived from experimental data and simulated structures: (a) ratio of average chord length of alumina grains to that of zirconia grains and (b) fraction of grain boundary area between alumina and alumina grains and alumina and zirconia grains, respectively.

derived from the respective Voronoi structure obtained after fitting the model to the experimental data. The ratios of average chord length of alumina grains to that of zirconia grains are in excellent agreement (Fig. 9a). The experimental grain boundary areas between grains of equal or unequal phases correspond well to the areas obtained for the model structures (Fig. 9b). Since the volume fractions of the phases have the highest priority in fitting of the structures they agree always within 0.5% to the experimental volume fractions. This demonstrates that a very good description of the experimental microstructure is obtained by the fitted model structures.

The FEM simulation of thermal conductivity and Young's modulus for these structures is shown in Fig. 10. The simulated data have been corrected due to residual porosity in the ZTA ceramics (compare Table 2) by the procedure described in the previous paragraph. Simulated thermal conductivities are in reasonable agreement (Fig. 10a), whereas the simulated Young's moduli are in excellent agreement to the experimental data. Small differences between measured and simulated thermal conductivities are attributed to the small model. So the statistical accuracy can be further improved by considering more grains.

5. Conclusions

For the representation of bi-continuous ceramic microstructures, two different models are used. The infiltration ceramic is modelled by a simple cubic structure which allows the selective variation of microstructure parameters, e.g. the contact area between agglomerates. The ZTA ceramic is represented best by fitting a modified Voronoi structure to the experimental structure. A good agreement between experimental and simulated composite properties is obtained. The generation and simulation of the cubic structures (Fig. 3) is very fast. However, the accurate reproduction of the microstructure by Voronoi polyhedra requires the generation of many test structures. Therefore, future work will concentrate on increasing the efficiency of this procedure.

The advantages of establishing accurate tools for microstructure–property simulations have been demonstrated with the two examples of the present paper. After validation of the model considerably more information is available about the microstructure than obtained from experimental analysis, e.g. the stress distribution. Therefore, additional design criteria for composite development may be derived.

Acknowledgements

The present study was supported by Fraunhofer-Gesellschaft within a joint project on multiscale modelling of materials (MAVO MMM). The authors acknowledge the help of H. Schömig and M. Römer with the analysis of the ZTA samples.

References

1. Hashin, Z., The elastic moduli of heterogeneous materials. *J. Appl. Mech.*, 1962, **29**, 143–150.
2. Hill, R., Elastic properties of reinforced solids: some theoretical principles. *J. Mech. Phys. Solids*, 1963, **11**, 357–372.
3. Miloh, T. and Beneviste, Y., A generalized self-consistent method for the effective conductivity of composites with ellipsoidal inclusions and cracked bodies. *J. Appl. Phys.*, 1988, **63**, 789–796.
4. Boccaccini, A. R. and Fan, Z., A new approach for the Young's modulus-porosity correlation of ceramic materials. *Ceram. Int.*, 1997, **23**, 239–245.
5. Boccaccini, A. R., Ondracek, G., Mazilu, P. and Windelberg, D., On the effective Young's modulus of elasticity for porous materials: microstructure modelling and comparison between calculation and experimental values. *J. Mech. Behav. Mater.*, 1993, **2**, 119–128.
6. Chu, Y. C. and Rokhlin, S. I., Effective elastic moduli of fiber-matrix interphases in high-temperature composites. *Metall. Mater. Trans.*, 1996, **27a**, 165–182.
7. Hale, D. K., The physical properties and composite materials. *J. Mater. Sci.*, 1976, **11**, 2105–2141.
8. Hashin, Z. and Shtrikman, S., A variational approach to the theory of the elastic behaviour of multiphase materials. *J. Mech. Phys. Solids*, 1963, **11**, 127–140.
9. Torquato, S., Random heterogeneous media: microstructure and improved bounds on effective properties. *Appl. Mech. Rev.*, 1991, **44**, 37–46.
10. Jefferson, G., Haritos, G. K. and McMeeking, R. M., The elastic response of a cohesive aggregate—a discrete element model with coupled particle interaction. *J. Mech. Phys. Solids*, 2002, **50**, 2539–2575.
11. Scherer, G. W., Calas, S. and Sempéré, R., Densification kinetics and structural evolution during sintering of silica aerogel. *J. Non-Cryst. Solids*, 1998, **240**, 118–130.
12. Raether, F. and Iuga, M., Effect of particle shape and arrangement on thermoelastic properties of porous ceramics. *J. Eur. Ceram. Soc.*, in press.
13. Raether, F., Meinhardt, J., Klimera, A. and Ruska, J., Microstructure design and heat flow in thin ZTA substrates for the electronics industry. In: Symp. A Materials Development for Microelectronic Devices. Material Week 2000, Munich, Germany, 2000, www.materialsweek.org.
14. Raether, F., Durschang, B. and Thiel, N., Microstructural design of a CAD/CAM machinable infiltration ceramic with high strength and near net shape performance. In: Symp. M, Ceramics. Material Week 2002, Munich, Germany, 2002, www.materialsweek.org.
15. Exner, H. E. and Hougardy, H. P., *Quantitative image analysis of microstructures*. DCM Informationsgesellschaft Verlag, 1988.
16. Gogotsi, G. A., Zavada, V. P. and Swain, M. V., Mechanical property characterization of a 9 mol% Ce-TZP ceramic material. I. Flextural response. *J. Eur. Ceram. Soc.*, 1995, **15**, 1185–1192.
17. Gellatly, B. J. and Finney, J. L., Characterization of models of multicomponent amorphous metals: the radical alternative to the Voronoi polyhedron. *J. Non-Cryst. Solids*, 1982, **50**, 313–329.
18. Green, D. J., Hannink, R. H. and Swain, M. V., *Transformation Toughening of Ceramics*. CRC Press, Inc., 1989.
19. Dörre, E. and Hübner, H., Alumina-processing, properties and applications. *Material Research and Engineering*. Springer-Verlag, 1984.
20. Raether, F., Hoffman, R., Müller, G. and Soelter, H. J., A novel thermo-optical measuring system for the in situ study of sintering processes. *J. Therm. Anal.*, 1998, **53**, 717–735.